1   **Titanium dioxide-Polyaniline/Silk fibroin microfiber sensor for**

2   **pork freshness evaluation**

3   Yongqiang Shi[a, &], Zhihua Li[a, &], Jiyong Shi[a, c, &], Fang Zhang[a], Xucheng Zhou[a], Yahui
4   Li[a], Mel Holmes[b, c], Wen Zhang[a], Xiaobo Zou[a, c, *]
5   a School of Food and Biological Engineering, Jiangsu University, Zhenjiang 212013,
6   China
7   b School of Food Science and Nutrition, the University of Leeds, Leeds LS2 9JT,
8   United Kingdom
9   c Joint Laboratory of China-UK on food nondestructive sensing, Jiangsu University,
10   Zhenjiang 212013, China
11   [&] The first three authors contributed equally.
12   * Corresponding author. Tel: +86 511 88780085; Fax: +86 511 88780201
13   Email address: zou_xiaobo@ujs.edu.cn (Xiaobo Zou)

14   **Abstract:**

15   A novel and low-cost micro-sensor with a diameter of 12 μm was developed
16   based on Titanium dioxide-Polyaniline/Silk fibroin fiber (TiO_2-PANI/SFF).
17   TiO_2-PANI composites were deposited on surfaces of SFFs by in-situ polymerization.
18   The microfibers were characterized by Scanning electron microscopy (SEM), Energy
19   dispersive spectrometer (EDS), Raman spectrometer, Fourier transform infrared
20   (FTIR) spectroscopy and X-ray diffraction (XRD), and the formation mechanism of
21   them was illustrated in detail. With ammonia (NH_3) as model gas, the TiO_2-PANI/SFF
22   micro-sensor showed good sensing performance with response value of 0.82 and
23   response time of 10 s to NH_3 of 100 μg/L. When the micro-sensors were applied for
24   pork freshness evaluation, the output response values showed good correlation with
25   the total volatile basic nitrogen (TVB-N) levels in pork (R^2=0.990), and the
26   discriminant results of the micro-sensors for pork freshness based on linear
27   discriminant analysis (LDA) showed the prediction accuracy of calibration and
28   prediction set was 90.73% and 86.38%, respectively, which indicated the great
29   potential of TiO_2-PANI/SFF micro-sensor for pork freshness evaluation.

32

1. Introduction

Achieving accurate and rapid detection of meat freshness is one of the major challenges for meat industry [1]. Quality of pork decreases rapidly during transportation and storage because of bacterial growth and enzymatic actions [2, 3], which may cause poor food taste or even food poisoning. The traditional methods for evaluating pork freshness include sensory test, chemical analysis and viable bacterial counts [4-6]. Sensory test is a rapid method, but it's not reliable when meat freshness changes slightly. Both chemical analysis and viable bacterial counts are objective methods, but they are time-consuming and couldn't be competent with modern industrialization process. Therefore, development of new fast, low-cost and accurate method for evaluation of pork freshness is of great significance.

Gas sensing technology has been playing an increasingly important role due to their promising applications in many fields such as medical diagnosis, monitoring of environmental pollutants and human health and safety [7-9]. Moreover, it could be applied to the evaluation of meat freshness. Volatile amines, including ammonia, histamine, tyramine, tryptamine and putrescine, etc., are produced by protein decomposition of pork because of microbial spoilage and biochemical reactions [10, 11]. These volatile amines constitute the total volatile basic nitrogen (TVB-N) which are closely related to meat freshness [6]. It might be possible to relate the freshness of pork with the concentration of volatile amines so as to make prepared sensors as indicators to evaluate pork freshness. There have been several studies attempting to marry meat freshness with the presence or concentration of certain substance emitted by meat [12-14]. For example, Cheuk-Fai Chow et al. [15] successfully applied Re(I)-Pt(II) sensor to detect CH_3SCH_3 in real rotten pork with a linear luminometric response up to 20.0 $mg \cdot kg^{-1}$ (R = 0.997) and the detection limit as 0.05 $mg \cdot kg^{-1}$. Naomi Funazaki et al. [16] presented a semiconductor gas sensor based on Rh-La_2O_3-In_2O_3 showing excellent sensitivity and selectivity to ethyl acetate produced in the initial bacterial putrefaction of meat at 300 °C. These studies confirmed the reliability of gas sensors for assessing freshness of meat. However, the prepared sensors based on these studies are often complicated to fabricate, high cost or environmentally harmful as the rare metal was used in their sensors. Therefore, it is highly desirable to develop a micro-size, cost-effective and eco-friendly sensor for the evaluation of meat freshness.

Polymer-metal oxide based composites have recently attracted extensive

attention due to their unique properties of catalytic activity [17], photocatalytic activity [18] and gas sensitivity [19]. Polyaniline (PANI), a kind of polymer with conjugated electronic structure, has been widely applied to the development of various devices on account of its good environmental stability and unique properties such as electrochemical, electroluminescence, redox behavior [20-22]. TiO_2, a typical n-type semiconductor, has also received extensive studies in gas detection because its electrical resistance has a strong dependence on the concentration of surrounding gases [23]. Previous study has reported gas-sensing performance of polymer-metal oxide (n-type) based sensor could be greatly improved owing to the P-N junction presenting in their backbones [24]. Accordingly, the synergetic effect of TiO_2-PANI may show great gas-sensing property over conventional sensors based on nanometal oxides. Unfortunately, the applications of polyaniline based sensors are restricted for poor mechanical property and low processability of polyaniline [17].

Natural silk provides a way to solve the above problems due to its excellent characteristics. Natural silks produced by silkworm have unique structure as shown in the supplementary information (Fig. S1 (a) and (b)), Silk fibroin fiber and sericin protein are the main components of natural silk [25]. Owing to the water solubility of sericin protein, natural silks have to be degummed before use. As shown in Fig.S1 (c) and (d), silk fibroin fiber contains a large number of amino acid residues providing great potential for surface modification of silk fibroin fiber [26, 27], and the past reports have confirmed that the main components of silk peptides could be endowed with a great number of in situ active sites [28, 29]. In addition, silk fibroin fibers in size of about 10 μm not only ensure the convenience for further processing and assembly, but also meet the needs for miniaturization. Therefore, silk fibroin fiber provides a great potential for the fabrication of low-cost and micro-size gas sensor.

The aim of this study is to develop a cost-effective and eco-friendly microfiber sensor for ammonia detection and pork freshness evaluation. TiO_2-PANI nanocomposites were firstly deposited on the surfaces of silk fibroin fibers by in-situ polymerization. The obtained composites were characterized in detail and then applied as the gas sensors. The performances of the prepared TiO_2-PANI/SFF micro-sensors were evaluated by detecting ammonia gas at room temperature. Finally, the prepared sensors were applied to evaluate pork freshness.

2. Experimental

100 *2.1. Materials*

101   Cocoons of silkworm were supplied by Zhejiang textile Co., Ltd. (China).

102 Sodium carbonate (Na_2CO_3, 99.8%), P25 titanium dioxide powder (TiO_2, 95%),

103 sulfuric acid (H_2SO_4, 98%), ammonium persulfate (APS, 98%), trimethylamine

104 (TMA, 33%) and ammonium hydroxide ($NH_3 \cdot H_2O$, 25~28%) were purchased from

105 Sinopharm Chemical Regent Co., Ltd. (China). Aniline was purchased from Aladdin

106 Chemical Reagent Co., Ltd and distilled under reduced pressure before use. High

107 purity air was purchased from Jiangsu Thorpe Co., Ltd. (China). Fresh pork was

108 bought from Auchan supermarket. (Zhenjiang, China). Double distilled water was

109 used to prepare all solutions.

110 *2.2. Preparation of TiO_2-PANI/SFF sensor*

111 *2.2.1. Preparation of silk fibroin fibers*

112   Silk fibroin fibers were obtained by degumming method removing the sericin

113 proteins from silkworm cocoons. The degumming process was carried out through

114 boiling the cocoons in 0.05 M Na_2CO_3 solution for half an hour. Then double distilled

115 water was used to wash the degummed SFFs thoroughly. The obtained SFFs were

116 dried in a vacuum at 40°C for 12h and stored in the dark at room temperature.

117 *2.2.2. Preparation of TiO_2-PANI/SFF microfiber*

118   TiO_2-PANI/SFF microfibers were prepared by in-situ polymerization technique.

119 Specifically, 0.15 g of SFFs were dispersed in 0.5 M H_2SO_4 solution (40 mL)

120 containing different amount of TiO_2 nanoparticles with magnetic stirring for 0.5 h,

121 followed by the addition of 182.4 μL of aniline dissolved in 0.5 M H_2SO_4 (10 mL)

122 with magnetic stirring for 20 min. Then the in-situ polymerization of aniline was

123 initiated by dropwise adding 0.456 g APS dissolved in 0.5 M H_2SO_4 (50mL) into the

124 above solution. The whole synthesis process was carried out in ice/water bath at 0 °C

125 for different hours with magnetic stirring. At last, the prepared composite was washed

126 and filtered for five times with distilled water and then dried for 12 h at 40 °C.

127 *2.3. Characterization*

128   The morphologies of composite microfibers were characterized using a scanning

129 electron microscope (SEM, S-4800, Hitachi, Japan). Energy scattering pattern were

130 obtained using X-max EDS spectrometer (Oxford, UK). Raman spectra were

131 investigated using a microscopic confocal Raman spectrometer with 532 nm laser

132 excitation (ThermoFisher, USA). The structure changes of prepared materials were
133 studied by a Thermo Scientific Nicolet iS50 FT-IR Spectrometer (ThermoFisher,
134 USA). The XRD patterns were obtained from a Rigaku Miniflex 600 powder
135 diffractometer (Cu Kα radiation, 40 kV 15 mA) with a D/Tex Ultra 250 1D CCD
136 detector.

137   The volume conductivity σ was calculated as follows [30]:

138 $$\sigma = \frac{4L}{\pi \square D^2 \square R} \tag{1}$$

139 Where σ, R, D and L is the conductivity (S/cm), resistance (Ω), diameter (cm) and
140 length (cm) of prepared fiber samples, respectively. The conductivity was calculated
141 by repeatedly measuring the resistance of samples five times via 2-probe method at
142 room temperature using a digital multimeter (Agilent 34410A, USA). The length (L)
143 of prepared fiber samples was 0.5 mm. The diameter of fibers was about 12 μm seen
144 from SEM morphologies of prepared materials.

145 *2.4. Fabrication of TiO$_2$-PANI/SFF micro-sensor*

146   A simple fabrication strategy was used to assemble TiO$_2$-PANI/SFF micro-sensor.
147 Briefly, conductive silver adhesive was utilized to weld a single composite microfiber
148 onto both ends of positive and negative electrodes of a flexible flat cable (FFC,
149 spacing of 0.5mm) with the help of an optical microscopy. The photo of the FFC cable
150 and the details of the prepared sensor were shown in Fig. 1 (a), respectively.
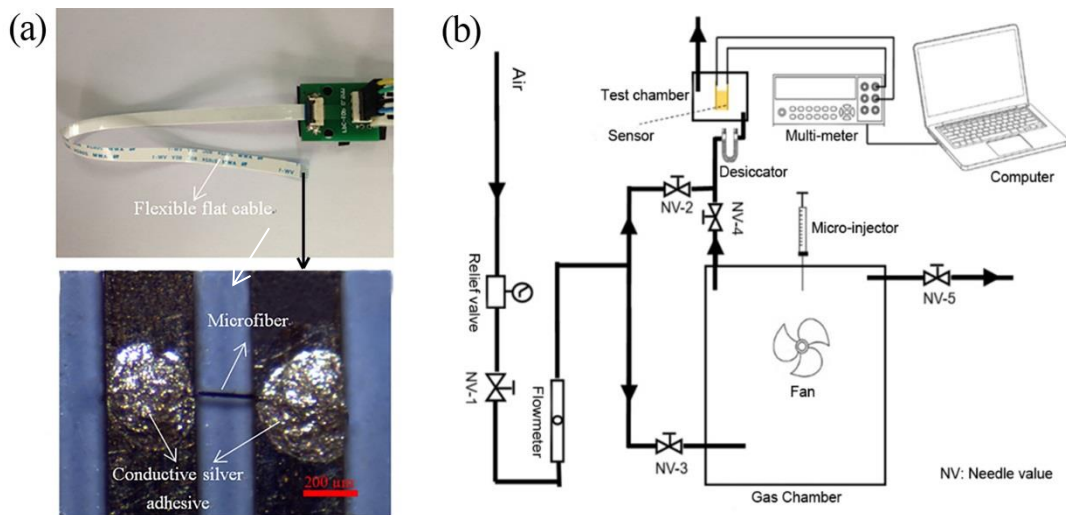
151

152 **Fig. 1** (a) the photo of the FFC cable and the details of the prepared micro-sensor; (b) Schematic diagram of
153 sensors' performance testing setup.

154 *2.5. Performance testing of the prepared micro-sensors*

155   Gas-sensing performances of the prepared micro-sensors were studied by a

home-made system at room temperature of 25 °C as shown in Fig. 1 (b). Teflon tubing was used as the connection pipeline. Pure air was employed to vent 30 min at a speed of 2 L/min to purify the whole test device before testing. During the test, a certain amount of liquid volatile ammonia was injected into the gas chamber by using a micro-injector, and then the fan was opened for 2 h to make injected liquid evaporate completely and mix evenly. Mixed gases could enter into the test chamber by controlling switching state of the needle valves. Resistance of a sensor was measured by a multimeter at 2 s intervals.

The concentration of ammonia in gas phase was controlled by controlling the injection amount. The concentration of target gas was calculated by the following formula [31],

$$C = \frac{22.4 * \rho * d * V_1}{M * V_2} \tag{2}$$

where C (ppm) is the target gas concentration, ρ (g/mL) is the density of the liquid, d is the purity of the liquid, V_1 (μL) is the volume of the liquid, V_2 (L) is the volume of the glass chamber, and M (g/mol) is the molecular weight of the liquid.

The response value of sensor was defined as:

$$S = \frac{R - R_0}{R_0} \tag{3}$$

Where R is the resistance when the sensor was exposed to testing gases, R_0 is the resistance of the sensor in pure air.

2.6. Evaluation of pork freshness

In order to examine the feasibility of the fabricated TiO_2-PANI/SFF micro-sensors, a piece of fresh pork was cut into pieces of 10 g, and then they were stored separately in test chambers at 4 °C. In the following seven days, two parts of pork samples were prepared to test response values of the sensor and determine the content of TVB-N in pork every day, respectively. TVB-N, as a traditional indicator of pork freshness, could well reflect the degree of protein decomposition in pork [6, 32]. Response values of the prepared micro-sensors were measured by a home-made system as shown in Fig. S2 (a), and the test steps of pork freshness evaluation was illustrated in detail in the document of "Supplementary Material". TVB-N content in pork was determined by a steam distillation method according to the previous

186   literature [33]. All results are the average value of five times repetition to same
187   sample. The correlation between the response values and TVB-N contents was fitted
188   through the curve fitting to verify the correlation between them. Linear Discriminant
189   Analysis (LDA), constructing discriminant functions through linear combination of
190   labeled data, is one of the most widely used supervised classification procedure [34].
191   In this study, LDA was applied to verify the feasibility of the prepared micro-sensor
192   used in the prediction of pork freshness.

3. Results and discussion

3.1. Characterization of TiO$_2$-PANI/SFF microfiber

195   Morphologies of the silk fibroins coated with different nanomaterials including
196   PANI, TiO$_2$-PANI were characterized by SEM images. As shown in Fig.2 (a), the
197   uncoated silk fibroins possessed quite smooth surfaces, and the diameters of silk
198   fibroins were about 12 μm. Fig.2 (b) showed the surface morphology of silk fibroin
199   deposited with PANI. It can be observed there existed polyaniline lamellar structure
200   on the surface of silk fibroin. The growth of polyaniline layer may result from the
201   large number of amino acid residues of silk fibroins seizing the aniline monomer or its
202   polymer through hydrogen bonding and ionic bond. Fig.2 (c) and (d) were the SEM
203   images of TiO$_2$-PANI/SFFs prepared by controlling the reaction time of 2 h and TiO$_2$
204   amount of 0.025 g. The doping of TiO$_2$ had a significant effect on morphologies and
205   structures of the microfibers. The smaller TiO$_2$ nanoparticles were agglomerated in the
206   presence of polyaniline, forming larger TiO$_2$-PANI composite particle clusters. A large
207   number of polyaniline filaments with diameter of about 20 nm extended from the
208   surface of particle clusters, which could be a boost for binding the particle clusters to
209   the surfaces of silk fibroins. At last these particle clusters were randomly distributed
210   on the surfaces of silk fibroins, forming a layer of TiO$_2$-PANI composite with a large
211   specific surface area.
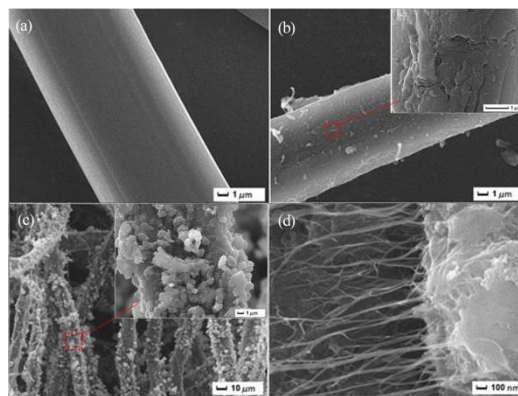
212 **Fig. 2** SEM images of (a) SFF, (b) PANI/SFF, and (c-d) TiO2-PANI/SFF.

213   The incorporation of TiO_2 nanoparticles on the polyaniline substrate was verified

214 by energy dispersive spectrum (EDS). As seen in Fig.3 (a), the titanium peak in the

215 spectrum confirmed the successful modification of TiO_2 onto polyaniline substrate.

216 The functional groups vibration of the composites was characterized by laser Raman

217 spectroscopy in Fig.3 (b). The characteristic peaks at 1163 and 1491 cm^{-1} are

218 attributed to the stretching vibration of C=N double bond of quinoid structure from
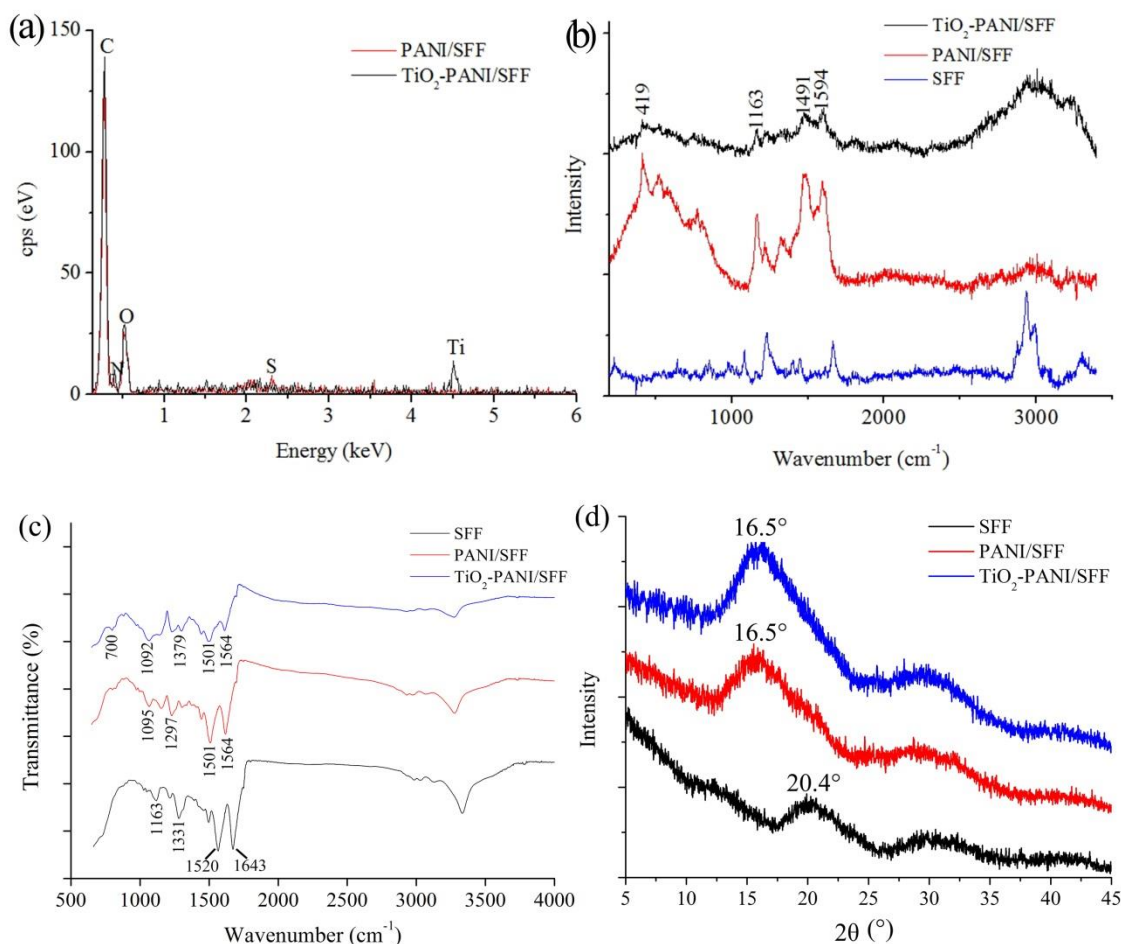
219 PANI [35]. The peaks at 419 and 1594 cm^{-1} exhibited the presence of benzene ring in

220 PANI [36, 37]. However, these peaks were not obvious in the silk fibroins spectra,

221 which confirmed the existence of polyaniline in the prepared composites.

222 **Fig. 3** (a) EDS, (b) Raman spectra, (c) FTIR spectra and (d) XRD patterns of SFF, PANI/SFF and TiO2-PANI/SFF.

223   The structure changes of prepared materials were studied by FTIR spectroscopy.

224 As Fig.3 (c) shows, the characteristic peaks for pure SFF occurs at 1643 cm^{-1} (amide

225 I), 1520 cm^{-1} (amide II), 1331 cm^{-1} (amide III), 1163 cm^{-1} (amide IV), indicating the

226 existence of β -sheet structure in SFF [38]. The main characteristic FTIR spectra of

227 PANI/SFF shows the band at 1564 and 1501 cm^{-1} ascribed to C＝C and C＝N

8

228 (stretching vibrations of benzenoid and quinoid rings) of PANI, while a band at 1297

229 cm^{-1} is attributed to C－N stretching vibrations of benzenoid unit and that at 1095

230 cm^{-1} is assigned to C－O stretch [39]. TiO$_2$-PANI/SFF exhibits spectral information

231 similar to that of PANI/SFF. Remarkably, the peak for both amide I and amide II in

232 TiO$_2$-PANI/SFF move to lower wave number (1564 cm^{-1} and 1501 cm^{-1}), which

233 indicate that polyaniline has some interactions with peptide linkages in SFF

234 macromolecular chains[40].

235 Fig.3 (d) shows the XRD patterns of three types of fibers (SFF, PANI/SFF,

236 TiO$_2$-PANI/SFF). Obviously the characteristic diffraction peak for the degummed

237 fibers occurs at 2θ = 20.4°, which are corresponding to the β-sheet structures in silk II

238 fibroin of SFF[41]. Compared with SFF, PANI/SFF and TiO$_2$-PANI/SFF show fairly

239 large shifts in position of diffraction peak, confirming that the interaction of

240 polyaniline with the peptide linkages in SFF macromolecular chains[40]. According

241 to the previous work [40, 42, 43], hydrogen-bonding interactions between peptide

242 linkages and hydrogen atom on nitrogen atoms of PANI are considered to be main

243 interactions to anchor the PANI on SFFs while the electrostatic attraction may play a

244 secondary role.

245 According to the above analysis, the mechanism of TiO$_2$-PANI/SFF preparation

246 was shown in Fig. 4. Firstly, the titanium dioxide was distributed uniformly in H$_2$SO$_4$

247 solution. When the aniline monomer and ammonium persulfate were added, the

248 aniline monomers were polymerized to form polyaniline on the surfaces of titanium

249 dioxide nanoparticles and silk fibroins, respectively. Then the titanium dioxide

250 nanoparticles coated with polyaniline were gradually agglomerated forming titanium

251 dioxide-polyaniline composite particles with diameter of about 2 μm. Meanwhile,

252 protonated amino groups of polyaniline backbones were combined with the amino

253 acid residues of silk fibroins, forming sheath structures on surfaces of silk fibroins.

254 After that, a large number of polyaniline filaments attached to silk fibroins were

255 further extended making the combination of TiO$_2$-PANI composite particles and silk

256 fibroins more stable.

257
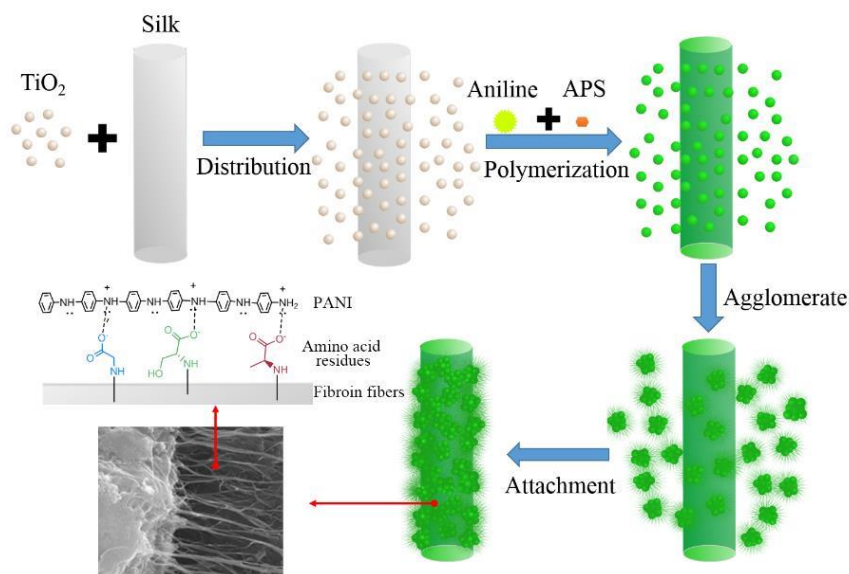
Fig. 4 The mechanism of TiO$_2$-PANI/SFF microfiber preparation.

3.2. Gas-sensing performance of TiO$_2$-PANI /SFF micro-sensor

3.2.1. Optimization of TiO$_2$-PANI /SFF micro-sensor

In order to obtain good gas-sensing performances of TiO$_2$-PANI/SFF micro-sensors toward volatile amines produced by pork spoilage, ammonia (NH$_3$) was selected as the simulation model gas to optimize performances of the prepared sensors. In this study, two variables were considered during the optimization, i.e. TiO$_2$ concentration and polymerization time.

Typical resistance transients of the TiO$_2$-PANI/SFF micro-sensor toward NH$_3$ were shown in Fig. 5 (a). When the sensor was exposed in NH$_3$ gas, dramatic resistance changes could be observed due to the deprotonation of polyaniline [44] as following : PANI-H$^+$ + NH$_3$ $\Leftrightarrow$ PANI + NH$_4^+$. When NH$_3$ gas was replaced with air, the resistance gradually returned to its original state. Fig. 5 (b) showed transients and changes of the response values of the TiO$_2$-PANI/SFF micro-sensors prepared respectively with 0.005 g, 0.015 g, 0.025 g and 0.05 g of TiO$_2$ toward 100 µg/L of NH$_3$. Clearly, response values of the sensors increased with TiO$_2$ amount rising from 0.005 g to 0.025 g, which may be ascribed to the synergies of the n-p junction presenting in the backbones between titanium dioxide and polyaniline. However, response values of the sensors decreased obviously with further increasing TiO$_2$ amount, which could be explained by the fact that excessive TiO$_2$ amount obstructed the bonding between the target gas and inner composites of the sensors. A conclusion from the Fig. 5 (b) could be drawn that the optimum amount of TiO$_2$ is 0.025 g for improving ammonia sensing performances.
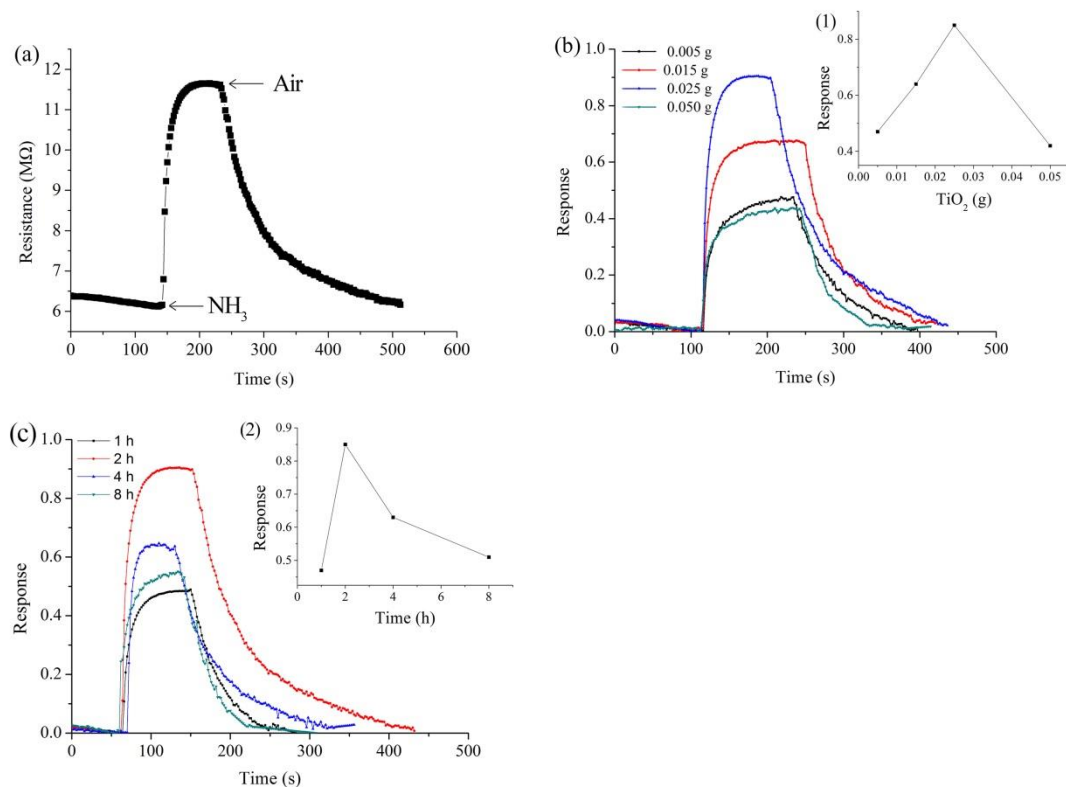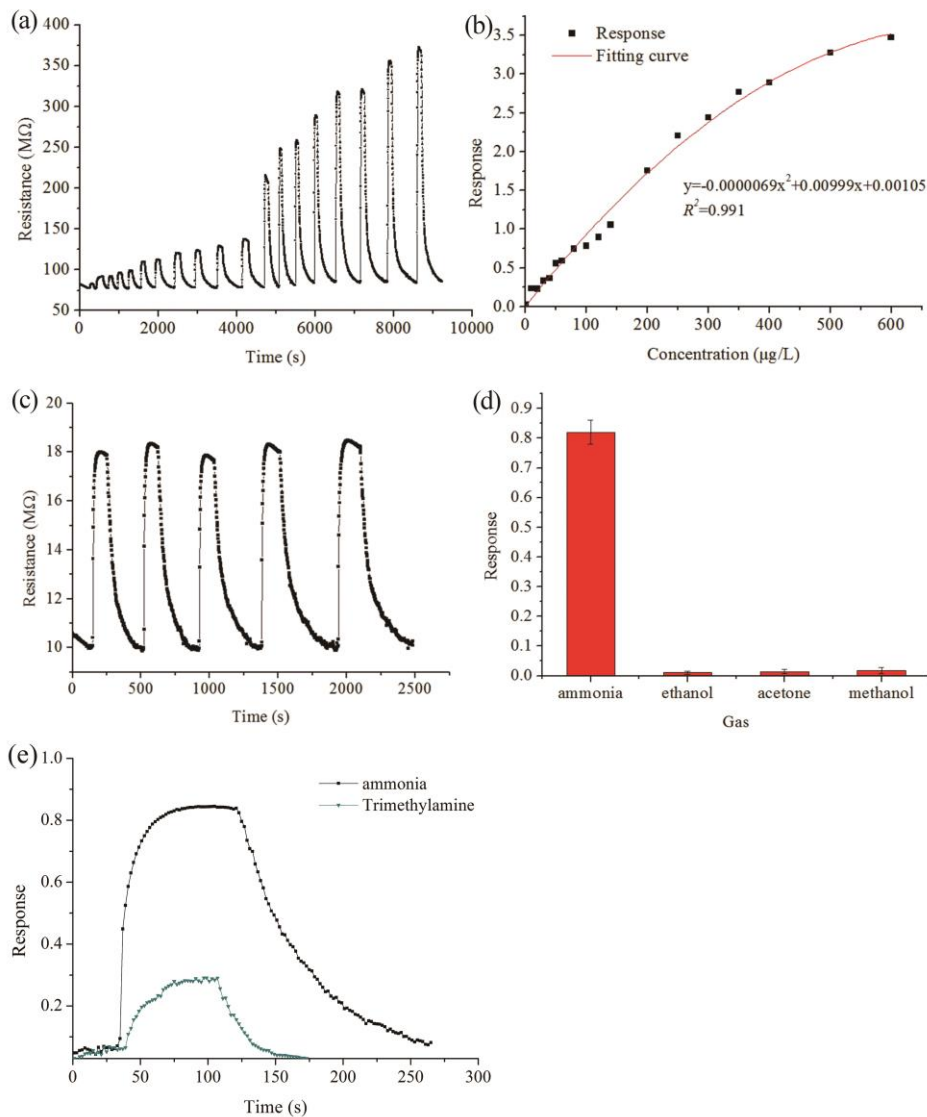
Fig. 5 (a) Typical resistance transients of the TiO₂-PANI/SFF micro-sensor toward NH₃; (b) Transients and inset (1) changes of the response values of the micro-sensors prepared respectively with 0.005g, 0.015g, 0.025g and 0.05g of TiO₂ to 100 μg/L of NH₃; (c) Transients and inset (2) changes of the response values of the micro-sensors prepared respectively with stirring time of 1h, 2h, 4h and 8h to 100 μg/L of NH₃.

The transients and changes of the response values of the TiO₂-PANI/SFF micro-sensors prepared respectively with stirring time of 1 h, 2 h, 4 h and 8 h toward 100 μg/L of NH₃ were shown in Fig. 5 (c). With stirring time extending from 1 h to 8 h, response values of the sensors increased first and then decreased. When stirring time was 2 h, the resultant TiO₂-PANI/SFF sensor exhibited the best sensing properties toward 100 μg/L of NH₃ compared to the others. The most likely reason is that an entire network of PANI is difficult to form on the surfaces of silk fibroins as polymerization time is short. The response values decreased obviously when stirring time was more than 2 h, which could be explained that the conjugated monomers are apt to form conductive particles in the solution instead of attracting unceasingly on the surface of fibers with polymerization time prolonged [40]. The conductivities of obtained materials were measured to support the view. The results measured were: $3.16*10^{-6}$, $7.37*10^{-2}$, $5.83*10^{-4}$ and $9.21*10^{-5}$ S/cm for 1, 2, 4 and 8 h, respectively. It can be seen that the conductivities of the TiO₂-PANI/SFF composites were the best while the polymerization time was two hours, which support the validity of the conjecture.

3.2.2. Ammonia sensing performance

302   Fig. 6 (a) showed resistance transients of the TiO$_2$-PANI/SFF micro-sensor
303   versus ammonia in the concentrations of 5-600 μg/L under the optimum conditions at
304   25 °C. The prepared micro-sensor showed good response-recovery characteristic.
305   When the sensor was exposed to ammonia, the resistance increased rapidly and
306   eventually reached equilibrium, the response time was about 10 s. When exposed in
307   the air, resistance of the sensor gradually returned to baseline, the recovery time was
308   about 280 s. Fig. 6 (b) showed response values of the sensor with ammonia
309   concentration   increasing.   The   regression   equation   is
310   y=-0.0000069x^2+0.00999x+0.00105 （R^2=0.991）. The summary table about
311   performance of reported PANI based sensors and the comparison between them and
312   our work was included in Table 1. Compared to reported works, the prepared sensor
313   has the advantages of faster response, wider detection range and speedy recovery.

Fig. 6 (a) Resistance transients and (b) response values of the TiO$_2$-PANI/SFF micro-sensor exposed to NH$_3$ of

different concentration at 25 °C; (c) Resistance transients of the micro-sensor to 100 μg/L of NH$_3$ for five times; (d)

Response values of the micro-sensor to several common reducing gases at 25 °C; (e) Response transients of the

same sensor to both ammonia and trimethylamine with the same concentration of 100 μg/L.

Table 1. Response (S), response time (T_1), recovery time (T_2), studied detection range (D_R), materials (M) and measured temperature (T_M) of the various NH$_3$ gas sensors.

Materials	S	T_1 (s)	T_2(s)	D_R（ppm）	T_M (°C)	Authors
TiO$_2$-PANI/SFF	0.82(100 ppm)	10	280	5-600	25	This paper
PANI	0.96 (100 ppm)	122	1235	10–100	25	G.D.Khuspe et al.[45]
PANI-PSSA/TiO$_2$	0.81(100 ppm)	60	120	10-100	25	QianqianLin et al.[46]
CSA-PANI/SnO$_2$	0.91(100 ppm)	46	3245	10-100	30	G.D. Khuspe et al.[47]
PANI/rGO	0.59(50 ppm)	-	240	5-50	25	X Huang et al.[48]
S, N: GQDs/PANI	0.42(100 ppm)	115	44	1-1000	25	J.N.Gavgani et al.[49]
PANI/TiO$_2$	1.67(23 ppm)	18	58	23-141	25	Tai et al.[50]
PANI/TiO$_2$	<0.5(100 ppm)	41	>500	20-100	25	SG Pawar et al.[51]
PANI/SnO$_2$	0.72(100 ppm)	>180	>420	10-100	25	G.D.Khuspe et al.[52]

3.2.3. Repeatability, stability and selectivity of TiO$_2$-PANI/SFF micro-sensor

For practical application, reliability of a gas sensor depends largely on the repeatability and stability of itself. Fig. 6 (c) showed resistance transients of the prepared sensor toward 100 μg/L of NH$_3$ for five times. From the resultant figure, each response curve was basically similar, and the resistance could be restored to initial state after each round of testing. The relative standard deviation of response values for five times was 3.14% indicating great repeatability of the prepared sensor. Subsequently, the stability of same sensor toward 100 μg/L of NH$_3$ was studied for a month. The results showed response value of the sensor was reduced to 88.1% of its initial value after the 30th day indicating relatively long-term stability.
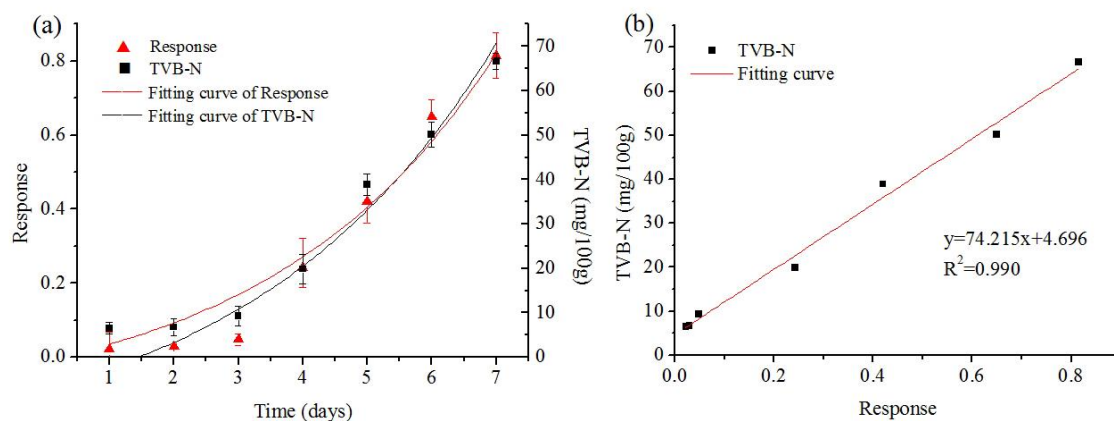
Excellent selectivity in detection of a target gas with presence of multiple gases is another critical parameter. Several common reducing gases, including ammonia, ethanol, acetone and methanol, were employed for testing response values of the

333   prepared micro-sensor at room temperature as shown in Fig. 6 (d). The concentration
334   of each tested gas was kept at 100 µg/L. Clearly, the response value to ammonia was
335   0.82 while the sensor has little response to the other gases indicating high selectivity
336   of the prepared sensor toward ammonia gas.

337   It is reported that some toxic small molecular components will be produced
338   during storage of pork meat, such as ammonia, hydrogen sulfide, trimethylamine,
339   etc.[53]. Therefore, Trimethylamine, as a contrast to ammonia, was chosen to test
340   performance of the prepared sensor. Fig.6 (e) shows the response transients of the
341   same sensor to both ammonia and trimethylamine with the same concentration of 100
342   µg/L. Seen from Fig.6 (e), the prepared sensor has response of 0.29 to trimethylamine
343   while the response to ammonia is more than 0.8, indicating that the sensor has a
344   certain response to amines, but is more sensitive to ammonia.

345   *3.3. Application of TiO$_2$-PANI/SFF micro-sensor in pork freshness evaluation*

346   Fig. 7 (a) showed the changes of TVB-N contents and response values of the
347   prepared micro-sensor to pork samples with prolonged storage time. Seen from the
348   graph, the sensor response values and TVB-N content had no obvious changes in the
349   first three days, and then both of them increased exponentially with further prolonging
350   storage   time   of   pork.   The   nonlinear   fitting   equations   were
351   y=0.178*exp(x/3.823)-0.260 (R^2=0.966) and y=11.240*exp(x/3.559)-12.0 (R^2=0.967),
352   respectively. According to Chinese standard GB/T 5009.44, 2003 [33], TVB-N
353   content less than 15 mg/100g was regarded as fresh meat, content in 15-25 mg/100g
354   as the second and more than 25 mg/100g as spoiled meat. Obviously, pork of the first
355   three days was judged as fresh meat, its quality was on the decline in the fourth day,
356   and the meat had been spoiled on the fifth day, which was consistent with response
357   values of the sensor. Furthermore, Dependence of TVB-N for pork samples on the
358   corresponding response values was shown in Fig. 7 (b), it can be found a good linear
359   relationship between them, the regression equation is y=74.215x+4.696 (R^2=0.990).

Fig. 7 (a) the changes of TVB-N contents and response values of the micro-sensor to the samples with prolonged storage time. (b) Dependence of TVB-N contents for pork samples on the corresponding sensor response values.

Linear discriminant analysis (LDA) was employed to verify the feasibility of the prepared micro-sensor used in the prediction of pork freshness. All the samples data were randomly divided into calibration and prediction dataset in the ratio of 2:1 used for building the discriminant models. The results obtained showed that the prediction accuracy of calibration and prediction set was 90.73% and 86.38%, respectively, which indicated the prepared micro-sensor had potential for pork freshness evaluation.

4. Conclusions

A novel TiO_2-PANI/SFF micro-sensor was proposed for pork freshness evaluation with the characteristics of easy fabrication, low cost, environment friendly and miniaturization. With ammonia as the model gas, the micro-sensor showed good sensing performance with response value of 0.82 and response time as short as 10 s to NH_3 of 100 μg/L. When the micro-sensor was applied to pork freshness evaluation, a well linear relationship (R^2=0.990) was found between output response values and TVB-N levels in pork, and the discriminant results of the micro-sensor for pork freshness based on linear discriminant analysis (LDA) showed the prediction accuracy of calibration and prediction set was 90.73% and 86.38%, respectively. The excellent performance of TiO_2-PANI/SFF sensor benefited from the porous and ultra-thin hairy structure. In conclusion, the proposed TiO_2-PANI/SFF micro-sensor holds great promise in the application of pork freshness evaluation.

Figure Captions

Fig. 1. (a) The photo of the FFC cable and the details of the prepared micro-sensor; (b) Schematic diagram of sensors' performance testing setup.

Fig. 2. SEM images of (a) SFF, (b) PANI/SFF, and (c-d) TiO$_2$-PANI/SFF;

Fig. 3. (a) EDS, (b) Raman spectra, (c) FTIR spectra and (d) XRD patterns of SFF, PANI/SFF and TiO$_2$-PANI/SFF.

Fig. 4. The mechanism of TiO$_2$-PANI/SFF microfiber preparation.

Fig. 5. (a) Typical resistance transients of the TiO$_2$-PANI/SFF micro-sensor toward NH$_3$; (b) Transients and inset (1) changes of the response values of the micro-sensors prepared respectively with 0.005g, 0.015g, 0.025g and 0.05g of TiO$_2$ to 100 μg/L of NH$_3$; (c) Transients and inset (2) changes of the response values of the micro-sensors prepared respectively with stirring time of 1h, 2h, 4h and 8h to 100 μg/L of NH$_3$.

Fig. 6 (a) Resistance transients and (b) response values of the TiO$_2$-PANI/SFF micro-sensor exposed to NH$_3$ of different concentration at 25 °C; (c) Resistance transients of the micro-sensor to 100 μg/L of NH$_3$ for five times; (d) Response values of the micro-sensor to several common reducing gases at 25 °C; (e) Response transients of the same sensor to both ammonia and trimethylamine with the same concentration of 100 μg/L.

Fig. 7. (a) The changes of TVB-N contents and response values of the micro-sensor to the samples with prolonged storage time. (b) Dependence of TVB-N contents for pork samples on the corresponding sensor response values.

Table 1. Response (S), response time (T1), recovery time (T2), studied detection range (DR), materials (M) and measured temperature (TM) of the various NH3 gas sensors.

References

[1] J.A.V. Albelda, A. Uzunoglu, G.N.C. Santos, L.A. Stanciu, Graphene-titanium dioxide nanocomposite based hypoxanthine sensor for assessment of meat freshness, Biosensors and Bioelectronics, 89, Part 1(2017) 518-524.

[2] X. Qiu, D. Itoh, T. Satake, H. Suzuki, Microdevice with integrated multi-enzyme sensors for the measurement of pork freshness, Sensors and Actuators B: Chemical, 235(2016) 535-540.

[3] M. Ingram, R.H. Dainty, Changes Caused by Microbes in Spoilage of Meats, Journal of Applied Microbiology, 34(2008) 21-39.

[4] N. Kaneki, T. Miura, K. Shimada, H. Tanaka, S. Ito, K. Hotori, et al., Measurement of pork freshness using potentiometric sensor, Talanta, 62(2004) 215-219.

[5] X. Guo, F. Huang, H. Zhang, C. Zhang, H. Hu, W. Chen, Classification of traditional Chinese pork bacon based on physicochemical properties and chemometric techniques, Meat Science, 117(2016) 182-186.

[6] H. Li, Q. Chen, J. Zhao, M. Wu, Nondestructive detection of total volatile basic nitrogen (TVB-N) content in pork meat by integrating hyperspectral imaging and colorimetric sensor combined with a nonlinear data fusion, LWT - Food Science and Technology, 63(2015) 268-274.

[7] L. Zhang, R. Dong, Z. Zhu, S. Wang, Au nanoparticles decorated ZnS hollow spheres for highly improved gas sensor performances, Sensors and Actuators B: Chemical, 245(2017) 112-121.

[8] W. Zhang, S. Wang, Y. Wang, Z. Zhu, X. Gao, J. Yang, et al., ZnO@ZnS core/shell microrods with enhanced gas sensing properties, Rsc Advances, 5(2014) 2620-2629.

[9] P.-J. Chien, T. Suzuki, M. Tsujii, M. Ye, K. Toma, T. Arakawa, et al., Bio-sniffer (gas-phase biosensor) with secondary alcohol dehydrogenase (S-ADH) for determination of isopropanol in exhaled air as a potential volatile biomarker, Biosensors and Bioelectronics, 91(2017) 341-346.

[10] X. Hong, J. Wang, Discrimination and Prediction of Pork Freshness by E-nose: Springer Berlin Heidelberg; 2011.

[11] Q. Huang, Q. Chen, H. Li, G. Huang, Q. Ouyang, J. Zhao, Non-destructively sensing pork's freshness indicator using near infrared multispectral imaging technique, Journal of Food Engineering, 154(2015) 69-75.

[12] C. Rukchon, A. Nopwinyuwong, S. Trevanich, T. Jinkarn, P. Suppakul, Development of a food spoilage indicator for monitoring freshness of skinless chicken breast, Talanta, 130(2014) 547-554.

[13] X. Hong, J. Wang, Z. Hai, Discrimination and prediction of multiple beef freshness indexes based on electronic nose, Sensors and Actuators B: Chemical, 161(2012) 381-389.

[14] X. Tian, J. Wang, S. Cui, Analysis of pork adulteration in minced mutton using electronic nose of metal oxide sensors, Journal of Food Engineering, 119(2013) 744-749.

[15] C.-F. Chow, P.-Y. Ho, D. Sun, Y.-J. Lu, W.-L. Wong, Q. Tang, et al., Development of sensitive and selective food sensors using new Re(I)-Pt(II) bimetallic complexes to detect volatile biogenic sulfides formed by meat spoilage, Food Chemistry, 216(2017) 382-389.

[16] N. Funazaki, A. Hemmi, S. Ito, Y. Asano, Y. Yano, N. Miura, et al., Application of semiconductor gas sensor to quality control of meat freshness in food industry, Sensors and Actuators B: Chemical, 25(1995) 797-800.

[17] M. Chen, M. Wang, Z. Yang, X. Wang, High performance and durability of order-structured cathode catalyst layer based on TiO2@PANI core-shell nanowire arrays, Applied Surface Science, 406(2017) 69-76.

461   [18] X. Chen, H. Li, H. Wu, Y. Wu, Y. Shang, J. Pan, et al., Fabrication of TiO2@PANI nanobelts with
462 the enhanced absorption and photocatalytic performance under visible light, Materials Letters,
463 172(2016) 52-55.

464   [19] T. Goto, T. Hyodo, T. Ueda, K. Kamada, K. Kaneyasu, Y. Shimizu, CO-sensing Properties of
465 Potentiometric Gas Sensors Using an Anion-conducting Polymer Electrolyte and Au-loaded Metal
466 Oxide Electrodes, Electrochimica Acta, 166(2015) 232-243.

467   [20] S. Pandey, Highly sensitive and selective chemiresistor gas/vapor sensors based on
468 polyaniline nanocomposite: A comprehensive review, Journal of Science: Advanced Materials and
469 Devices, 1(2016) 431-453.

470   [21] A. Eftekhari, L. Li, Y. Yang, Polyaniline supercapacitors, Journal of Power Sources, 347(2017)
471 86-107.

472   [22] J. Yukird, T. Wongtangprasert, R. Rangkupan, O. Chailapakul, T. Pisitkun, N. Rodthongkum,
473 Label-free immunosensor based on graphene/polyaniline nanocomposite for neutrophil
474 gelatinase-associated lipocalin detection, Biosensors and Bioelectronics, 87(2017) 249-255.

475   [23] R.K. Sonker, B.C. Yadav, Development of Fe2O3–PANI nanocomposite thin film based sensor
476 for NO2 detection, Journal of the Taiwan Institute of Chemical Engineers.

477   [24] H. Tai, X. Xu, Z. Ye, C. Liu, G. Xie, Y. Jiang, P–P heterojunction sensor of self-assembled
478 polyaniline nano-thin film/microstructure silicon array for NH3 detection, Chemical Physics Letters,
479 621(2015) 58-64.

480   [25] O. Hakimi, D.P. Knight, F. Vollrath, P. Vadgama, Spider and mulberry silkworm silks as
481 compatible biomaterials, Composites Part B: Engineering, 38(2007) 324-337.

482   [26] G. Li, H. Liu, T. Li, J. Wang, Surface modification and functionalization of silk fibroin
483 fibers/fabric toward high performance applications, Materials Science and Engineering: C, 32(2012)
484 627-636.

485   [27] J. Xu, H. Su, J. Han, Y. Chen, W. Song, Y. Gu, et al., In situ deposition of flower-like ZnO on silk
486 fibroin fibers, Applied Physics A, 108(2012) 235-238.

487   [28] H. Su, J. Han, Q. Dong, J. Xu, Y. Chen, Y. Gu, et al., In situ bioinspired synthesis of silver
488 chloride nanocrystals on silk fibroin fibers, Applied Physics A, 102(2011) 429-434.

489   [29] J. Liu, X. Zhang, H. Pang, B. Liu, Q. Zou, J. Chen, High-performance bioanode based on the
490 composite of CNTs-immobilized mediator and silk film-immobilized glucose oxidase for glucose/O2
491 biofuel cells, Biosensors and Bioelectronics, 31(2012) 170-175.

492   [30] M. Qu, F. Nilsson, Y. Qin, G. Yang, Y. Pan, X. Liu, et al., Electrical conductivity and mechanical
493 properties of melt-spun ternary composites comprising PMMA, carbon fibers and carbon black,
494 Composites Science and Technology, 150(2017) 24-31.

495   [31] L. Liu, P. Song, Z. Yang, Q. Wang, Highly sensitive and selective trimethylamine sensors based
496 on WO3 nanorods decorated with Au nanoparticles, Physica E: Low-dimensional Systems and
497 Nanostructures, 90(2017) 109-115.

498   [32] X. Huang, X. Zou, J. Zhao, J. Shi, X. Zhang, Z. Li, et al., Sensing the quality parameters of
499 Chinese traditional Yao-meat by using a colorimetric sensor combined with genetic algorithm partial
500 least squares regression, Meat Science, 98(2014) 203-210.

501   [33] U. Khulal, J. Zhao, W. Hu, Q. Chen, Intelligent evaluation of total volatile basic nitrogen
502 (TVB-N) content in chicken meat by an improved multiple level data fusion model, Sensors and
503 Actuators B: Chemical, 238(2017) 337-345.

[34] M. Xu, L. Ye, J. Wang, Z. Wei, S. Cheng, Quality tracing of peanuts using an array of metal-oxide based gas sensors combined with chemometrics methods, Postharvest Biology and Technology, 128(2017) 98-104.

[35] M. Trchová, Z. Morávková, M. Bláha, J. Stejskal, Raman spectroscopy of polyaniline and oligoaniline thin films, Electrochimica Acta, 122(2014) 28-38.

[36] Z. Morávková, J. Stejskal, M. Trchová, Spectroscopic study of the highly homogeneous polyaniline film formation on gold support, Spectrochimica Acta Part A: Molecular and Biomolecular Spectroscopy, 152(2016) 294-303.

[37] D.C. Ferreira, J.R. Pires, M.L. Temperini, Spectroscopic characterization of oligoaniline microspheres obtained by an aniline-persulfate approach, Journal of Physical Chemistry B, 115(2011) 1368-1375.

[38] H.T. And, Mitsuhiro Miyazawa, Molecular Orientation Behavior of Silk Sericin Film as Revealed by ATR Infrared Spectroscopy, Biomacromolecules, 6(2005) 2049.

[39] Z. Zhang, M. Wan, Y. Wei, Highly Crystalline Polyaniline Nanostructures Doped with Dicarboxylic Acids, Advanced Functional Materials, 16(2006) 1100-1104.

[40] Y. Xia, L. Yun, Fabrication and properties of conductive conjugated polymers/silk fibroin composite fibers, Composites Science and Technology, 68(2008) 1471-1479.

[41] Y. Iridag, M. Kazanci, Preparation and characterization of Bombyx mori silk fibroin and wool keratin2006.

[42] D. Gh, D. Kong, J. Gautrot, S.K. Vootla, Fabrication and Characterization of Conductive Conjugated Polymer-Coated Antheraea mylitta Silk Fibroin Fibers for Biomedical Applications, Macromol Biosci, 17(2017).

[43] X. Yang, T. Dai, Y. Lu, Synthesis of novel sunflower-like silica/polypyrrole nanocomposites via self-assembly polymerization, Polymer, 47(2006) 441-447.

[44] G.M. do Nascimento, N.A. Pradie, Deprotonation, Raman dispersion and thermal behavior of polyaniline–montmorillonite nanocomposites, Synthetic Metals, 217(2016) 109-116.

[45] G.D. Khuspe, D.K. Bandgar, S. Sen, V.B. Patil, Fussy nanofibrous network of polyaniline (PANi) for NH3 detection, Synthetic Metals, 162(2012) 1822-1827.

[46] Q. Lin, Y. Li, M. Yang, Gas sensing properties of layer-by-layer self-assembled ultrathin film of polyaniline/titanium dioxide, Synthetic Metals, 162(2012) 2242-2249.

[47] G.D. Khuspe, S.T. Navale, M.A. Chougule, R.N. Mulik, P.R. Godse, S. Sen, et al., NH3sensor based on CSA doped PANi-SnO2nanohybrid, 2014, pp. 925-926.

[48] X. Huang, N. Hu, R. Gao, Y. Yu, Y. Wang, Z. Yang, et al., Reduced graphene oxide–polyaniline hybrid: Preparation, characterization and its applications for ammonia gas sensing, Journal of Materials Chemistry, 22(2012) 22488-22495.

[49] J.N. Gavgani, A. Hasani, M. Nouri, M. Mahyari, A. Salehi, Highly sensitive and flexible ammonia sensor based on S and N co-doped graphene quantum dots/polyaniline hybrid at room temperature, Sensors and Actuators B: Chemical, 229(2016) 239-248.

[50] H. Tai, Y. Jiang, G. Xie, J. Yu, X. Chen, Fabrication and gas sensitivity of polyaniline–titanium dioxide nanocomposite thin film, Sensors and Actuators B: Chemical, 125(2007) 644-650.

[51] S.G. Pawar, M.A. Chougule, S.L. Patil, B.T. Raut, P.R. Godse, S. Sen, et al., Room Temperature Ammonia Gas Sensor Based on Polyaniline-TiO$_{2}$ Nanocomposite, IEEE Sensors Journal, 11(2011) 3417-3423.

547   [52] G.D. Khuspe, S.T. Navale, D.K. Bandgar, R.D. Sakhare, M.A. Chougule, V.B. Patil,
548   SnO2nanoparticles-modified polyaniline films as highly selective, sensitive, reproducible and stable
549   ammonia sensors, Electronic Materials Letters, 10(2014) 191-197.
550   [53] L. Huang, J. Zhao, Q. Chen, Y. Zhang, Nondestructive measurement of total volatile basic
551   nitrogen (TVB-N) in pork meat by integrating near infrared spectroscopy, computer vision and
552   electronic nose techniques, Food Chemistry, 145(2014) 228-236.
553
554